Use of superparamagnetic temperature transition measurement in nanocrystalline alloys to determine low crystalline fractions by modeling of the weak-coupling behavior

Nicolas Boust, Olivier Geoffroy, Herve Chazal, Sebastien Flury, Thierry Waeckerle, Alain Demier, Bashar Gony, James Roudet

Version of Record: https://www.sciencedirect.com/science/article/pii/S0304885318327136
Manuscript_566b1dd7cfa75feceb3b44340197bf30

Use of superparamagnetic temperature transition measurement in nanocrystalline alloys to determine low crystalline fractions by modeling of the weak-coupling behavior

Authors:

Nicolas Boust [1,2]

Olivier Geoffroy[1]

Hervé Chazal[1]

Sébastien Flury[1]

Thierry Waeckerlé[3]

Alain Demier [3]

Bashar Gony[2]

James Roudet[1]

[1]: Univ. Grenoble Alpes, CNRS, Grenoble INP, G2Elab, 38000 Grenoble, France

[2]: Aperam Alloys Amilly, 45200 Amilly France

[3]Aperam Alloys Imphy, 58160 Imphy France

Corresponding Author: Nicolas Boust: nicolas.boust@g2elab.grenoble-inp.fr

1. Introduction

Finemet type nanocrystalline soft magnetic alloys feature vanishing effective anisotropy, allowing thus to shape their hysteresis curve by inducing controlled anisotropy through field or stress annealing. Whereas the induced anisotropy K_u develop in FeSi crystalline phase, the hysteretic loop analysis only measures the macroscopic anisotropy K_u^m. Crystalline fraction f_c has thus to be known in order to determine $K_u = K_u^m/f_c$. Our ultimate goal is to analyze how K_u is induced during the first stages of field crystallization annealing. We aim so to measure f_c of partially crystallized samples, i.e $f_c \leq 0.1$.

We exclude ***systematic*** use of RXD measurement because of its heaviness and its lack of precision on low crystalline state, due to the difficulty to separate amorphous phase and crystalline phase contributions. Concretely, dealing with XRD, f_c accuracy reported in [1] is 0.05, leading for instance to a relative uncertainty around 50% for $f_c = 0.1$.

Magnethotermic method allows to overcome amorphous phase contribution screening effect problem, as above the amorphous Curie temperature T_C^a, the spontaneous polarization is only due to the crystalline phase. In such situation, FeSi phase is characterized by superparamagnetic or nanograins weak coupling behavior, requiring thus strong static field as $\mu_0 H = 0.75\ T$ [2], $0{,}4\ T$ [3], $0{,}6T$ [4] [5], to counterbalance thermal agitation. Measurement methods such as VSM [5] and Faraday balance [2] [3] are used, leading to rather long measurement time. Another point is that samples featuring low f_c cannot be measured above 480 °C, to prevent pursuit of crystallization. The FeSi Curie temperature T_C, around 600 °C being not reachable, the composition of the crystalline phase cannot be determined either.

For all these reasons, we decide to use weak alternative field ($H_{max} \approx 500\ A/m$, frequency $f = 1Hz$), generated by a simple winding on the core under test, the polarization being simply obtained by secondary winding voltage integration. Another interesting point is that the toroid shape is the one involved for industrial annealings and used in applications. Hysteretic loops measurements at different temperatures allow to determine the temperature T_{tr} characterizing the entrance in the superparamagnetic regime [4], [6], [7], [8]. The originality of our work consists of the use of T_{tr} to determine f_c. T_{tr} yet depends on Si balance in $Fe_{1-y}Si_y$ phase, and grain size D, in addition to f_c. It is consequently necessary to know the dependency relations $y(f_c)$ and $D(f_c)$ to be able to determine f_c from T_{tr} measurement. In our case, these relations are obtained from data bases performed in Aperam Imphy Center Research by XRD measurement carried out on reference samples featuring $f_c \geq 0.13$. We report here the results of our investigations dealing with the modelling of weak coupling, experimental characterization of T_{tr}, and its use for determining f_c.

2. Modeling of the inter-nanograin weak coupling (dipolar interactions)

Experiment shows that in temperature span between T_c^a and T_{tr}, the inter-nanograin strong ferromagnetic coupling existing for $T < T_c^a$ is replaced by a residual weak coupling, allowing the material to keep an apparent ferromagnetic behavior. This weak coupling may be due to residual ferromagnetic exchange coupling between crystalline and amorphous phases, as proposed by Hernando [3], [7], [9], [10], [11] or to dipolar interactions [12] [13]. We studied the dipolar hypothesis in [14] in the frame of an accurate modelling, equations being partially remained here. This description will be completed in § 5 by integrating residual inter-phase ferromagnetic exchange coupling.

2.1 Principle and dipolar contribution to weak coupling formulation

In first approximation, the orienting field is the Lorentz field $H_L = f_c \langle J \rangle/(3\mu_0)$ with $\langle J \rangle = \left\| \langle \vec{J} \rangle \right\|$ the spatial average of instantaneous polarization. Macro-dipoles (MDs) $\vec{p} = V\,\vec{J}$ associated to nanograins, with V the nanograin volume, are considered. Angular MDs density probability law $\mathrm{P}(\theta)$ is determined by a Boltzmann statistic, function of the ratio between the magnetic energy $-\vec{p}\,\overrightarrow{H_L}$ and the thermic energy $k_B T$, i.e.

$$\mathrm{P}(\theta) \propto \exp\left(\frac{V\, J_S\, f_c\, \langle J\rangle\, \cos\theta}{3\,\mu_0\, k_B T}\right) \sin\theta$$

With, in this context, J_s the $FeSi$ phase spontaneous ferromagnetic polarization at the considered temperature.

The time average MD polarization $\left\|\vec{\bar{J}}\right\|$ (denoted $\bar{J}$ for simplicity) is thus obtained:

$$\frac{\bar{J}}{J_S} = \mathcal{L}\left[\frac{J_S\, V}{k_B\, T}\frac{f_c\, \langle J\rangle}{3\mu_0}\right] \qquad \mathcal{L} = \text{Langevin function} \qquad (1)$$

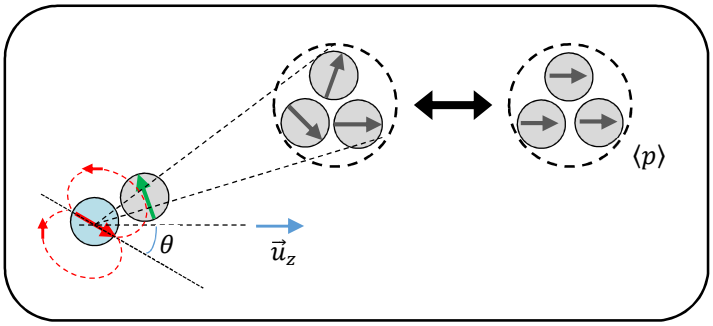

Fig. 1 : Illustration of the spatial averaging, authorized for distant MDs only. The field lines created by the central dipole are represented in red

Due to system ergodicity, $\bar{J} = \langle J\rangle$ and will both be denoted J_s^{wc} (subscript s as spontaneous, in the absence of applied field) by now. One obtains with (1)

$$\frac{J_s^{wc}}{J_S} = \mathcal{L}\left[\frac{J_S\, V}{k_B\, T}\frac{f_c\, J_s^{wc}}{3\mu_0}\right] \qquad (2)$$

Giving the transition temperature with this approximation T_{tr}^{Lo}

$$T_{tr}^{Lo} = \frac{f_c\, \pi\, D^3 J_s^{tr\,2}}{54\, \mu_0\, k_B} \qquad (3)$$

N.B. By now, the subscript or superscript tr indicates that the corresponding entity is evaluated at T_{tr}.

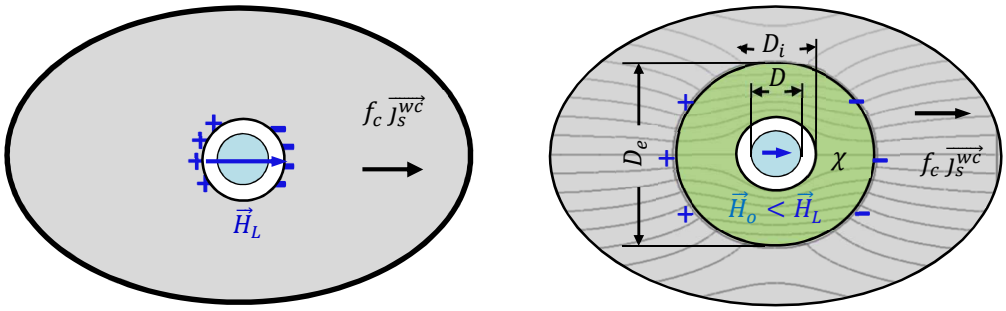

(a) (b)

Fig. 2: Screening effect on environment created field due to shell (right) compared to Lorentz approximation (left) (from [15]). The central MD is not represented

Measurements show that T_{tr}^{Lo} is overvalued, due to the irrelevant spatial averaging used to describe the close surroundings of a MD. In fact, the spatial averaging is relevant only if carried out on a group of several equivalent nanograins. Considered from the central MD, nanograins are equivalent if they (i) feature comparable distances to central MD and (ii) belong to the same angular sector, as qualitatively pitched by dashed lines on

Fig. 1. The problem is that, dealing with central MD neighbors, groups are made of only one nanograin –cf. green MD on Fig. 1-. In this case, spatial averaging is of course meaningless. A consequence of this operation is that the interactions between the central MD and its neighbors, leading to individual specific instantaneous orientations of each of them, are not rendered, with, as a result, an overestimated apparent energy of the configuration. The resulting bias being more pronounced for unfavorable orientations of the central MD (regarding the mean polarization direction), the weight of these directions is underestimated in the Boltzmann statistic, leading to an overestimated average polarization, when calculated under the Lorentz field assumption.This effect is taken into account in [14] by considering that the close neighboring of the MD acts as a shell characterized by a susceptibility χ, which will partially screen the Lorentz field and thus lower the average polarization, as wished according to the preceding paragraph conclusion. S denotes the screening factor, leading to the effective orienting field

$$\vec{H}_o = \vec{H}_L / S \tag{4}$$

Correcting (2) and (3) into

$$\frac{J_s^{wc}}{J_S} = \mathcal{L}\left[\frac{J_S\, V}{k_B\, T}\frac{f_c\, J_s^{wc}}{3\mu_0\, S}\right] \tag{5}$$

$$T_{tr} = \frac{f_c\, \pi\, D^3 {J_s^{tr}}^2}{54\, \mu_0\, k_B\, S_{tr}} \tag{6}$$

Ferromagnetic polarization is ruled by a Heisenberg type power law [2]

$$J_S(T) = J_H(1 - T/T_C)^{0.36} \tag{7}$$

Leading with (6) to

$$\frac{T_{tr}}{(1 - T_{tr}/T_C)^{0.72}} = \frac{f_c\, \pi\, D^3 {J_H}^2}{54\, \mu_0\, k_B\, S_{tr}} = C\, \frac{f_c\, D(nm)^3 {J_H}^2}{S_{tr}} \qquad C = \frac{10^{-27}}{54 \times 4\, 10^{-7}\, 1.3810^{-23}} = 3.355 \tag{8}$$

S is then determined by the system equilibrium study [14]. Relations will be denoted with adimensional reduced polarizations and fields: $\vec{j} = \vec{J}/J_S$, $\vec{h} = \mu_0\, \vec{H}/J_S$. According to [16 p. 58], one obtains

$$S = \frac{(3+\chi)(2\chi+3)}{9\,(\chi+1)} \tag{9}$$

We also indicate the expression of the equilibrium field $\overrightarrow{h_{sh}}$ experienced in the shell, resulting from two contributions $\vec{h}_{co}^{ca}$ and $\vec{h}_{co}^{r}$, given by

$$\vec{h}_{sh}^{ca}(r,\theta) = \frac{f_c\, j_s^{wc}}{3+\chi}\left(\vec{u}_z - \frac{\chi}{3+2\chi}\frac{{R_i}^3}{r^3}(2\,\cos\theta\;\vec{u}_r + \sin\theta\;\vec{u}_\theta)\right) \tag{10}$$

$$\vec{h}_{sh}^{r}(r,\theta_p) = \frac{1}{3+2\chi}\,\frac{R^3}{r^3}\left(2\,\cos\theta_p\;\vec{u}_r + \sin\theta_p\;\vec{u}_{\theta p}\right) \tag{11}$$

Where r denotes the distance to the center of central nanograin, θ and θ_p the angular coordinates in common use with polar reference axis with $\overrightarrow{J_S^{wc}}$ and $\vec{J}$ as polar axes.

In order to determine χ, a structure similar to Fig.2b is considered, but the linear surrounding medium extends now everywhere ($D_e \to \infty$). In this situation, the central MD magnetic behavior characterizes the surrounding medium properties, allowing to determine χ by studying the system reaction to an applied field $\vec{h}_{a\chi}$. In addition, to avoid confusion with the situation pictured on Fig.2b, parameters in this context will be subscripted by the letter χ. This leads to

$$j_\chi = \mathcal{L}[x_\chi] \qquad x_\chi = \frac{{J_S}^2\, V}{\mu_0\, k_B T}\, h_{o\chi} \tag{12}$$

With $h_{o\chi}$ the orienting field. According to [14] and [17 (5.11) p.25] in the context of dielectrics, $h_{o\chi}$ obeys

$$h_{o\chi} = \frac{3(\chi+1)}{2\chi+3}\, h_{a\chi} \tag{13}$$

One has to notice that the magnitude $h_{a\chi}$ has to reproduce the situation experienced in Fig.2b, where the shell is polarized by the proximate central MD, and the distant mean polarization $f_c\,\overrightarrow{j_s^{wc}}$. This point is crucial because the resulting $h_{a\chi}$ is too great to allow the use of the order 1 limited development carried out by Onsager [18]. In other words, the susceptibility determined here is only an amplitude susceptibility, depending of $h_{a\chi}$. The study, detailed in [14], leads to the three relations

$$\chi = \frac{3\,\mathcal{L}[x_\chi]}{x_\chi\,\omega - \mathcal{L}[x_\chi]} \qquad (14) \qquad with\ \ \omega = \frac{S}{3\,S_{tr}}\,\frac{J_S(T_{tr})^2}{{J_S}^2}\,\frac{T}{T_{tr}} \qquad (15)$$

$$(3+\chi)\,h_{a\chi} = f_c\,\omega\,x_\chi \qquad (16)$$

2.2 χ_{tr} and S_{tr} determination

At T_{tr}, j_s^{wc} cancels. Consequently the polarizing field is due to central MD only. Identifying $h_{a\chi}$ with the mean field experienced by the shell, this leads to

$$h_{a\chi} = \langle {}^{tr}h_{sh}^{r}\rangle_{\theta p} \qquad (17)$$

With (11), one obtains

$$h_{a\chi} = \frac{A}{3+2\chi_{tr}}\,\frac{R^3}{{r_c}^3} \qquad (18) \qquad \mathrm{A} = \frac{1}{2}\int_0^\pi \sqrt{1+3\cos^2\theta_p}\,\sin\theta_p\,d\theta_p\ = 1{,}38 \qquad (19)$$

A constant expresses the averaging in all θ_p direction under which the shell is seen from the central MD and r_c the characteristic distance used to calculate the field. As the surrounding medium is composed of particles, whose behavior is above all ruled by its part submitted to the most intense field, due to its monodomain state, we so choose to use $r_c = D_i/2 = R/\sqrt[3]{f_c}$ (D_i indicated on Fig. 2), leading with (18) to

$$h_{a\chi} = \frac{A}{3+2\chi_{tr}}\,f_c \qquad (20)$$

Which is injected in (16), with, in this context, χ_{tr} instead of χ. With (14), this leads to

$$A - x_\chi^{tr}/3 = \mathcal{L}[x_\chi^{tr}] \qquad (21)$$

Solving (21) leads to $x_\chi^{tr} = 2.36$, to $\chi_{tr} = 9.28$ with (14) and to $S_{tr} = 2.86$ with (9). Due to approximations used, this value is only a crude estimation, which yet can be used to comparison with experimental data.

3. Model / measurement confrontation

Confrontation between the model and published experimental data has already been reported partially in [14]. This work is completed here, by the adding of experimental data we obtained at G2Elab and structural data obtained by Aperam-Imphy research team.

As shown by (8), T_{tr} depends on f_c, J_H and T_c, which are themselves function of the Si balance y, and finally on grain size D. At first, we aim to determine experimentally a more accurate, than the theoretical evaluation obtained in § 2.2, the value of parameter S_{tr}. To do this, we'll use (8) with samples featuring known f_c, D and y. A difficulty is that experimental uncertainty on D is typically $\Delta\mathrm{D} = 1nm$ [1] [19], which corresponds to 8% for $D = 12nm$ and to 25 % considering D^3. Assuming that others uncertainties are comparably negligible, the resulting uncertainty on S_{tr} will be 25 % too. To reduce this amount, we'll collect a panel of numerous data, reducing by this way random uncertainties. Systematic bias will be eliminated in a second step.

Data collected in our environment use Nanophy® samples, (y, D) being obtained from data bases performed in Aperam Imphy Center Research, as explained in the introduction, T_{tr} being measured in G2Elab. Several phenomena happen at T_{tr} such as coercive field H_c and remanent polarization nullification, or Hopkinson peak on initial permeability [6], [20], as shown on [6] Fig.1(a). For our experimental measurement, T_{tr} is determined by the temperature at which H_c vanishes.

Fig 3a, 3b, 3c and 3d show the $H_c(T)$ measurements for Nanophy® samples with different annealing. The magnitudes and shapes are very comparable to those reported in [11]

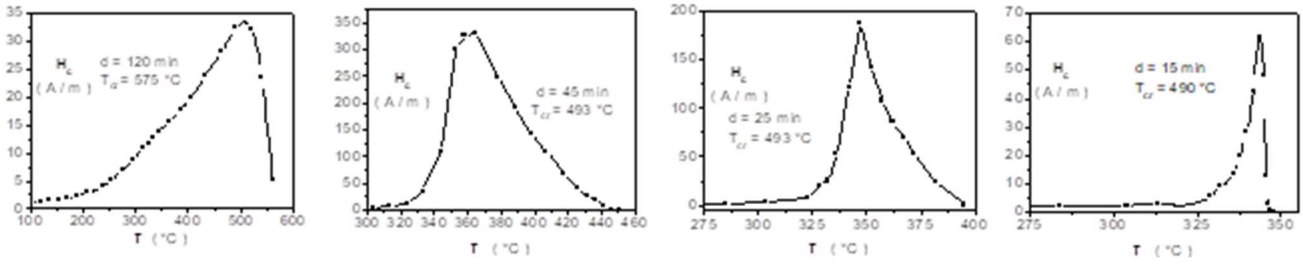

(a) *(b)* *(c)* *(d)*

Fig. 3: Coercive field according to the measurement temperature for different crystallization annealing temperature T_{cr} and duration d (Nanophy samples)

From the Aperam data base, analytical laws for $f_c(d, T_{cr})$ is obtained, with T_{cr} the annealing temperature and d its duration:

$$f_c = 0.756\left(1 - \left(\frac{\alpha}{\lambda_T\, d}\right)^{\beta}\right) \qquad \alpha = 1.405\ min \qquad \beta = 0.614 \qquad (22a)$$

$$\lambda_T = \exp(a - b/T) \qquad a = 58.17 \qquad b = 46594\ K \qquad (22b)$$

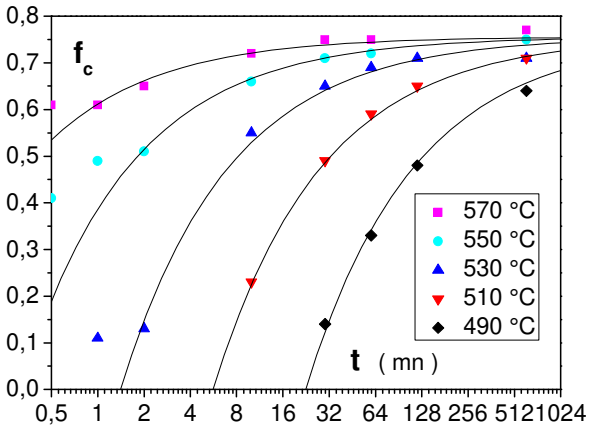

Fig. 4: Crystalline fraction obtained depending on annealing duration and temperature for Nanophys samples

Law (22b) corresponds to an Arrhenius law, with $k_B b = 4.02\ eV = 391\ kJ/mol$ the activation energy, matching the values reported in the literature [21], [22]. One has to take in mind that (22a) and (22b) do not work for $f_c < 0.13$, which corresponds to incubation phase presented in [23].

Same identification procedure has been carried out for $D(d,T)$ and $y(d,T)$. The adjusted analytical law $D(f_c)$ and $y(f_c)$ obtained are represented on Fig.5 and 6. Fig.6 curves show that annealing parameters have very little effect on $y(f_c)$ laws, making possible to use a unique law - the central curve, corresponding to $T_{cr} = 530\ °C$. The $y(f_c)$ drop after $y = 0.7$ corresponds to the total diffusion state [8], where all silicon is in the crystalline phase. In this situation, f_c increase corresponds to a silicon crystalline phase composition depletion. This effect is visible on the last Nanophy point on Fig.8.

Random uncertainty effects for D and y parameters for Nanophy® samples are thus eliminated. In order to eliminate the systematic bias, caused by experimental material and algorithms used to exploit data, we confronted the obtained D, y and T_{tr} (respectively Fig.9, 10 and 11) of Nanophy® samples to data from the literature for close composition alloys. For T_{tr} we considered only two of our four points, the ones corresponding to the fully crystalized sample and the one annealed 45 minutes, which feature a crystalline fraction known with

accuracy from kinetic laws (22a) and (22b), with $f_c > 0.13$. These samples are illustrated on Fig.3a and 3b and so will be denoted 3a and 3b from now. Literacy considered data are reported for 1h annealed at different temperature samples, with compositions given in Table 1. These data were published by Mazaleyrat and al [20], Herzer [8], Kulik and al [7].

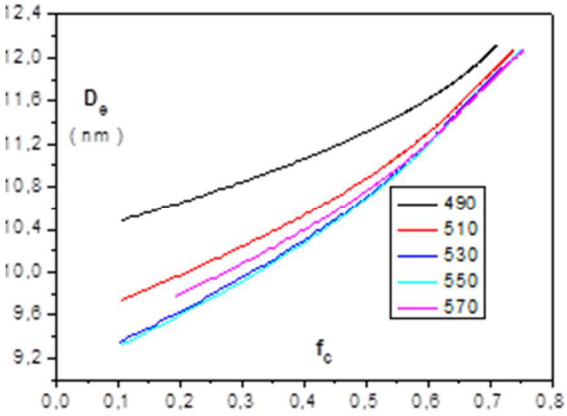

Fig. 5 : Nanograin average diameter depending on f_c and annealing temperature

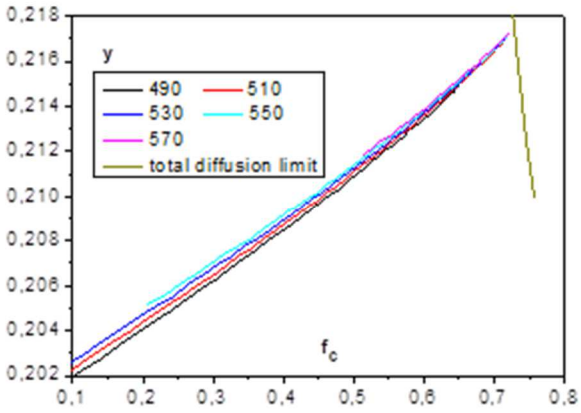

Fig. 6 Crystalline phase silicon content depending on $f_c$and annealing temperature

Source	Dénomination	Composition (at)
Aperam	Nanophy®	$Fe_{73.0}Cu_{1.1}Nb_{3.1}Si_{15.7}B_{7,1}$
[8]	Herzer	$Fe_{73.5}Cu_1Nb_3Si_{13.5}B_9$
[20]	Mazaleyrat	$Fe_{73.5}Cu_1Nb_3Si_{13.5}B_9$
[7]	Kulik	$Fe_{73.5}Cu_1Ta_3Si_{13.5}B_9$

Tab.1 samples compositions

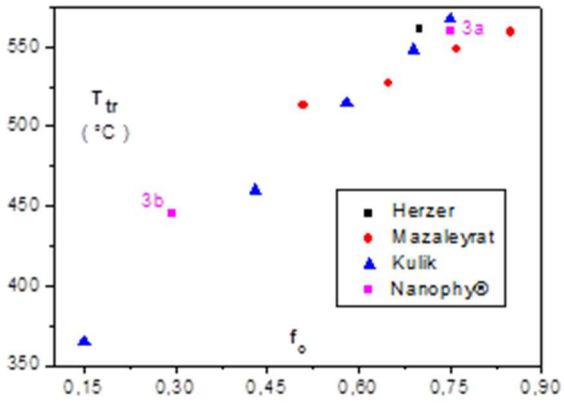

Fig.7 Transition temperature depending on f_c from various sources

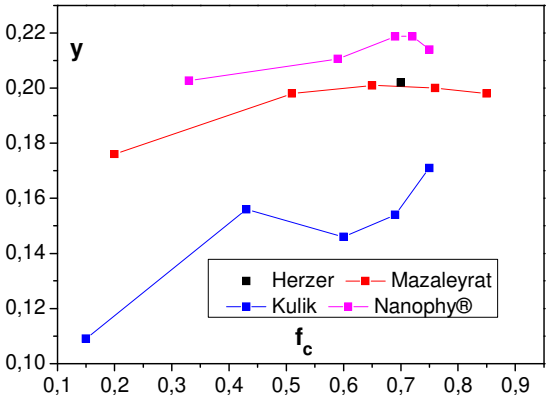

Fig.8: Crystalline phase silicon content depending on f_c from various sources

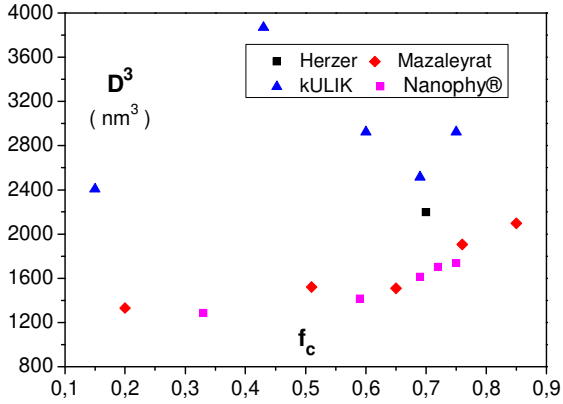

Fig.9: Nanograin diameter depending on f_c from various sources

T_{tr} data on Fig.7 show a shared behavior between all the families. Consequently, no matter the details of the model, one understands that for a given f_c value, D^3 and y variations from a family to another one have to balance their effects. According to (8) if D increases, y has to increases too.

Yet Kulik's data represented on Fig.8 and Fig.9 are the ones with the biggest grain size and lowest silicon content! Clearly, the global character of these inconsistencies demonstrates the existence of systematic bias, but the gap between its crystallographic data and other families is too big to allow to reconcile them with acceptable moderate systematic corrections. Dealing with other families, inconsistencies are moderate and systematic corrections are an option for reconcile them in the frame of simulating. Being unable to determine on which parameter (D , y or even f_c) the corrections have to be made, we decide to apply corrections only on D, whom experimental uncertainty is the more impacting, with 25% uncertainty on D^3, assuming $\Delta D = 1nm$ as seen above. For coherence, we decided that the corrections magnitude should not exceed 1nm too and adjust D and S_{tr} to fit as best as possible the points of Fig.9.

S_{tr} is determined from (8) with sample 3a ($T_{tr} = 833\ K$, $f_c = 0.75$) values. For this Nanophy sample, $y = 0.209$, value determined by applying the total diffusion criterion. One obtains $T_C = 872.5\ K$ $J_H = 1.82\ T$

Best fitting is obtained by increasing D by 8% for Nanophy® samples, reducing D by 3% for Mazaleyrat familly, and by 4% for Herzer unique point. Fig. 5 indicates $D_e(f_c = 0.75, T_{cr} = 570°C) = 12\ nm$, leading after correction to $D(f_c = 0.75, T_{cr} = 570°C) = 13\ nm$ and so $S_{tr} = 2.4$, given a 16% difference with the 2.86 modeled value. We consider that this difference is acceptable regarding model approximations.

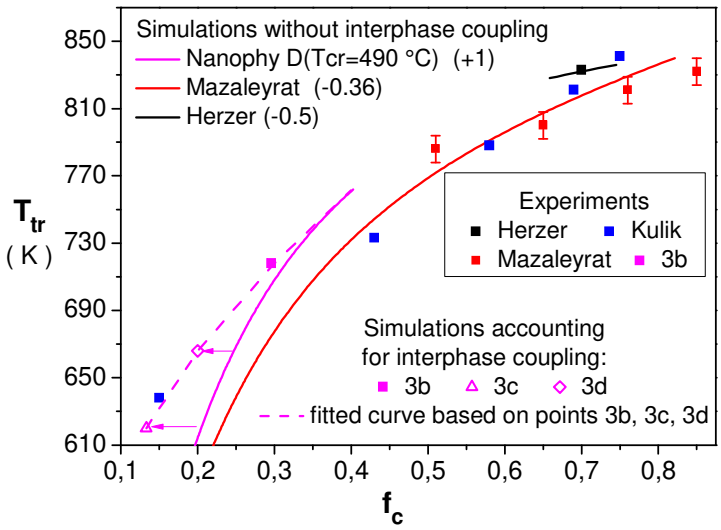

Fig. 10: Models/experiments confrontation. Systematic diameter corrections used for simulations are given in nanometers (values between brackets). The simulations accounting for interphase coupling use the same systematic correction. They are related to section 4

Concretely, in Nanophy®3b sample case, we use the $D(f_c)$ law for $T_{cr} = 490°C$, in black on Fig.5 , taking into account the 8% systematic correction indicated above, leading to:

$$D_{490}(nm) = 2 \times 1.08 \left(129 + 150\, f_c - 255\, {f_c}^2 + 319\, {f_c}^3\right)^{1/3} \qquad (23)$$

Analytical $y(f_c)$ law is adjusted according to Fig.6

$$f_c \leq 0.72 \qquad y = 0.201 + 0.01677\, f_c + 0.00763\, {f_c}^2 \qquad (24)$$

Structural laws being completed for Nanophy® samples, same process is carried out for Mazaleyrat data, leading to:

$$D = 0.97\left(11.05 - 0.973\, f_c + 3.57\, {f_c}^2\right) \qquad (23bis)$$

$$y = 0.151 + 0.149\, f_c - 0.1101\, {f_c}^2 \qquad (24bis)$$

Concerning Herzer's only point, with the previously mentioned corrective factor, following values are obtained:

$$D = 12.5\, nm \qquad (23ter) \qquad\qquad y = 0.20 \qquad (24ter)$$

Corresponding simulated curves are plotted on Fig.10 (continuous curves) and show good agreement with experimental points, validating thus the proposed model. In addition, one notices that the simulated curve based on Mazaleyrat's crystalline parameters (D and y) fits reasonably good Kulik's experimental points too. This fact should not be surprising, taking in mind that the two families were annealed with the same duration (one hour) and feature the same basic composition, except the replacement of Niobium (Mazaleyrat) by Tantale (Kulik), elements known to have equivalent effects. One simply notices that the range of crystalline fractions covered by Kulik's family is extended towards lower values, according to the corresponding range of annealing temperatures [480 °C, 580 °C], to be compared with the Mazaleyrat family range [525 °C, 625 °C] for the points reported here.

Nevertheless, it is visible that the first experimental point of Kulik ($T_{tr} = 637\ K, f_c = 0.15$) does not match with the simulated curve, the five points of Kulik suggesting and intriguing linear behavior, as previously noticed by Herzer [13], compared to the strong curvature featured by the simulated curve in the low f_c range. This question will be revisited at the end of section 4.

S_{tr} value and $y(f_c), D(f_c)$ relations being validated, it is now possible to use (8) for determining unknown f_c from T_{tr} measurement. We apply it for 3c and 3d Nanophy® samples, and denote f_c^{tr} crystalline fractions calculated in this frame. Values are compared in Table.2 to f_c^{kin} values, obtained with kinetic laws (19a) and (19b). Numerical values obtained for Nanophy®3b are also reported.

The 45 minutes annealing sample belonging to the samples panel used to adjust parameters, f_c^{tr} and f_c^{kin} logically match, as expected. Dealing with 3c and 3d samples, the f_c^{kin} values are outside the authorized range for applying kinetic laws, justifying our work, aiming to develop a reliable method for these samples. Nevertheless, the surprisingly relatively small variation of f_c^{tr} noticed comparing 3c and 3d intrigues us. Suspecting a bias in the modeling impacting the low f_c range, we will now evaluate the effect of a phenomenon neglected until now: amorphous and crystalline phase ferromagnetic coupling.

sample	$d\ (min)$	$T_{cr}\ (°C)$	$T_{tr}\ (°C)$	f_c^{kin}	f_c^{tr}	${}^{ex}f_c^{tr}$
3b	45	493	445	0.296	0.315	0.30
3c	25	493	393	0.095	0.25	0.20
3d	15	490	347	–	0.205	0.133

Tab. 2 Annealing time and temperature, transition temperature and calculated crystalline fractions for Nanophys samples

4. Amorphous and crystalline phase ferromagnetic coupling.

The main idea is that according to Hernando [3], [7], [9], [10], [11], even above T_C^a, a thin layer of the amorphous phase surrounding a nanograin is still ferromagnetically coupled with it. This phenomenon leads to an effective size $D_e > D$ regarding magnetic efficiency, as well as an effective crystallized fraction $f_c^e > f_c$. T_{tr} given, this phenomenon is expected to lead to actual value f_c smaller than the calculated f_c^{tr}.

This idea will be rendered here in the simple molecular field model frame. We consider that the rusticity of this approach is acceptable, dealing with the modeling of a corrective term. In the same vein, we'll consider an invariant composition for the crystalline phase, i.e. $Fe_{79.1}Si_{20.9}$, for quantitative evaluations.

4.1 General formulas

One writes the energy of the amorphous phase atomic magnetic moment $\overrightarrow{\mathcal{M}}$ as

$$U = -\overrightarrow{\mathcal{M}}\lambda_a(1 + \varepsilon\, {r_r}^{-n})\,\overrightarrow{J_s^a} \qquad\qquad r_r = r/p \tag{25}$$

With λ_a the intrinsic amorphous phase molecular field coefficient, p a characteristic distance of some angstrom related to the penetration depth. r roughly corresponds to the distance to the interface, ε being a constant quantifying the inter-phase contribution to coupling.

Dealing with the RKKY exchange interaction term, Skomski [24 p.272] indicates a power law with exponent n=3 to describe the decay of coupling interactions with distance. We arbitrary retain it in our context (while Hernando implements an exponential law in [10]). In fact, the detailed analytical expression is of little importance, the penetration depth being the relevant parameter. For convenience, we aim to normalize at 1 the value of the reduced distance r_r characterizing a point belonging to the interface. The distance r will be so counted from an origin located in the nanograin, distant of p from interface. We define the penetration depth considering that the interfacial coupling contribution obtained at the corresponding distance R reaches one tenth of its value at the interface, i.e. $(R/p)^3 = 10$, leading to $R = 2{,}15\ p$. The distance to the interface, i.e. the penetration depth, is so $R - p = 1.15\ p \cong p$.

Classical expressions are obtained, that is :

$$\frac{J_s^a}{J_0^a} = \mathcal{B}_J\left(\frac{J_0^a\ \lambda_a(1 + \varepsilon\ {r_r}^{-3})\ J_s^a}{N_a\ \mu_0\ k_B\ T}\right) \tag{26}$$

With J_0^a the spontaneous polarization at 0 K and N_a the volumetric concentration of magnetic atoms in amorphous phase, $\mathcal{B}_J$ being the Brillouin

$$\mathcal{B}_J(x) = \frac{2J+1}{2J}\coth\left(\frac{2J+1}{2J}x\right) - \frac{1}{2J}\coth\left(\frac{x}{2J}\right) \tag{27}$$

In the case of localized magnetism , J –not to be confused with polarization- describes the kinetic moment of the atom, but is rather a function, i.e. :phenomenological parameter here. $J = 1/2$ is usually used to describe thermomagnetical curve of Nickel, Iron and Cobalt [25 p. 69] and we consequently use this value. Resulting magnetothermic law for initial amorphous alloy (obtained by considering $\varepsilon = 0$ in (23)) is plotted on Fig.16.

(23) is expressed with $x = J_0^a\ \lambda_a(1 + \varepsilon\ {r_r}^{-3})\ J_s^a/(N_a\ \mu_0\ k_B\ T)$, leading to:

$$\frac{J_s^a}{J_0^a} = \mathcal{B}_{1/2}(x) \tag{28}$$

$$\frac{J_s^a}{J_0^a} = \frac{N_a\ \mu_0\ k_B\ T}{\lambda_a(1 + \varepsilon\ {r_r}^{-3})\ {J_0^a}^2}\ x \tag{29}$$

$${}^*T_C^a = \frac{\lambda_a\ {J_0^a}^2}{k_B\ N_a\ \mu_0} \tag{30}$$

The star in " ${}^*T_C^a$ " meaning the Curie temperature featured by the amorphous phase when isolated, this notation being originally introduced by Hernando [3]. By injecting (30) in (29), one obtains:

$$\frac{J_s^a}{J_0^a} = a\,x \qquad a = \frac{T}{{}^*T_C^a(1+\varepsilon\, r_r{}^{-3})} \tag{31}$$

In order to determine parameters ϵ and p values, an experimental reference magnetothermical curve $J_s^a(T)$ is needed. We will determine it with looking to the fully nanocrystallized sample.

4.2 Experimental determination of Nanophy® 3a sample $J_s^a(T)$ law

T_C^a is obtained by looking for an inflexion point on the magnetothermical law ${J_{exp}}^{1/0.36} = \mathrm{f}(T)$, following [4]. It is so obtained (cf. Fig. 11) $T_C^a = 262\ °C$. The characterization of $J_s^a(T)$ curve is completed writing:

$$J_s^a(T) = \frac{J_{exp}(T) - f_c\, J_s^c(T)}{1 - f_c} \qquad T < T_C^a \tag{32}$$

Note that the $Fe_{1-y}Si_y$ phase ferromagnetic spontaneous polarization is now denoted J_s^c, for symmetry with J_s^a, instead of J_s in § 2, when FeSi phase was alone. J_s denotes now the macroscopic spontaneous polarization, identified to J_{exp} for $T < T_C^a$.

As indicated in §3, $y = 0.209$ and $f_c = 0.75$.

One has to notice that for that for $T < 600\ K$, $J_s^c(T)$ is not ruled by an Heisenberg power law, as showed by our measurements carried out on massive $Fe_{79}Si_{21}$ sample (starred points on Fig. 12), with additional points (squared), after Fallot [26]. In the considered temperature span, the following law is obtained:

$$J_s(T) = J_s^0 - \gamma\, T - \delta\, T^4 \qquad J_s^0 = 1.47\ T \qquad \gamma = 2.148\ 10^{-4}\ T\ K^{-1} \qquad \delta = 1.089\ 10^{-12}\ T\ K^{-4} \tag{33}$$

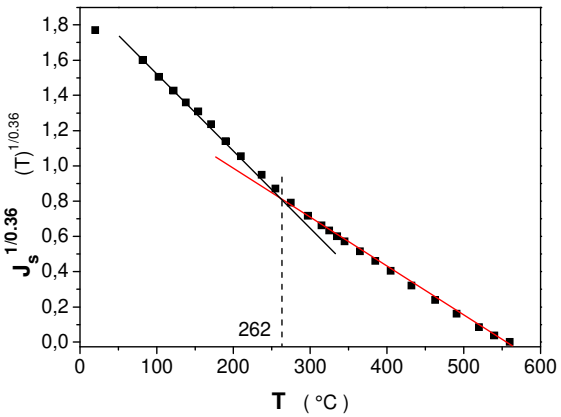

Fig. 11: experimental polarization at the power1/0.36 plotted in function of temperature. Inflexion point is noticeable at 262°C

With (33) the magnetothermic law $J_s^a(T)$ expressed by (32) is fully determined using experimental points $J_{exp}(T)$. Associated points are plotted in black on Fig.13. It is noticeable that the curve shape is deeply different from Heisenberg behavior, in contradiction with note [5] in [2], the same observation applying for Slawska results too ([27] Fig.2 curve 3). This is due to ferromagnetic exchange interactions coupling between amorphous phase and crystalline phase, Herzer's statement in [2] referring to isolated amorphous. Another noticeable point is that $J_s^a(T_{am}) \cong 0.71\ T$ is obtained from Fig.13, with T_{am} the ambient temperature, far above the $0.33\ T$ announced by Herzer [8] for a same composition alloy. This discrepancy is probably due to the fact that Herzer assumes an Heisenberg behavior until T_{am} to describe FeSi phase magnetic behavior (note [5] in [2]), overevaluating $J_s^c(T_{am})$, as shown on Fig. 12, and consequently underevaluating $J_s^c(T_{am})$.

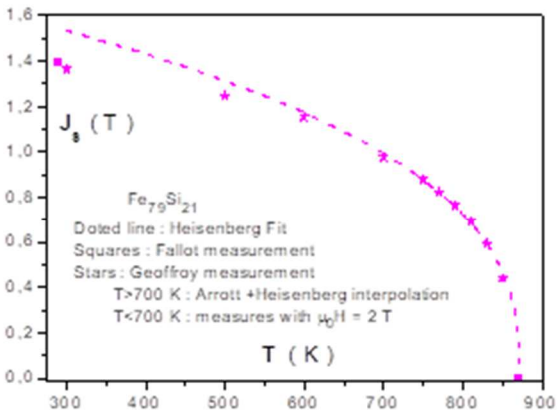

Fig. 12: Experimental measurement and simulated curve for $Fe_{79}Si_{21}$ polarization depending on temperature

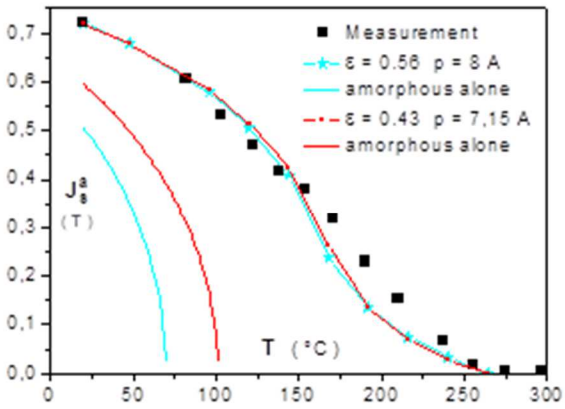

Fig. 13: Amorphous phase, alone or in nanocrystalline alloy, polarization curve depending on temperature

Parameters ε and p will now be determined using $J_s^a(T)$ curve.

4.3 ε and p determination for the fully crystallized state

According to (31) , $J_s^a(T)$ law is function of ε and p, but also of ${}^*T_C^a$, the Curie temperature of the amorphous phase alone, while Fig.13 only provides the Curie temperature of the amorphous phase intricated with FeSi phase. Yet it is possible to experimentally characterize an amorphous ribbon with the same composition than the residual amorphous phase to determine ${}^*T_C^a$. $y = 0.209$ and $f_c = 0.75$ known, and considering that copper atoms are in cluster, and thus not part of the amorphous phase, composition $Fe_{59.5}Nb_{11.7}B_{28.8}$ is obtained for final amorphous phase. Curie temperatures for two composition surrounding ours: $Fe_{63}Nb_9B_{28}$ and $Fe_{55}Nb_{12}B_{33}$, have been measured by Kuhrt [28], who obtains respectively ${}^*T_C^a = 90\,°C$, ${}^*T_C^a < T_{am}$.

Yet, Niobium being expelled of crystalline phase during grain growth and having very low diffusivity, the amorphous-crystalline phases interface in enriched in Niobium [29], and so the amorphous phase has lower Nb content than previously said. Effective composition is so $Fe_{(100-z)55/88}Nb_zB_{(100-z)33/88}$ with $z \in [4,12]$. Composition $z = 8$, obtained as powder by mechanical co-milling, is studied in [28], leading to ${}^*T_C^a = 70\,°C$. This value will be tested by keeping J_0^a as free parameter and the impact of ${}^*T_C^a$ choice will be illustrated by simulating also with ${}^*T_C^a = 100\,°C$.

One last effect has to be taken into account: in fully nanocrystallized alloy, distance Λ between adjacent grains (as denoted in [3]) is very little. Assuming for simplicity cubic shapes, according to [3], one obtains:

$$\Lambda = D_{eq}\left(f_c^{-1/3} - 1\right) \qquad {D_{eq}}^3 = \pi\, D^3/\,6 \tag{34}$$

With D_{eq} the length of the cubic grain featuring the same volume than a spherical one with diameter D. With $D = 13\,nm$ and $f_c = 0.75$, $\Lambda \cong 1.05\,nm$ is obtained. Due to this small value, neighboring nanograins influence areas overlap. Relation (29) has consequently to be adapted by the replacement:

$$r_r{}^{-3} \quad \rightarrow \quad r_r{}^{-3} + (\Lambda/p + 2 - r_r)^{-3} \tag{35}$$

Simulated curves of Fig. 13 and 14 will be obtained taking account of this point.

ε is determined by noticing that the most thermal agitation resilient regions are the interfaces, where the inter-phase coupling is maximum. Those regions determine thus T_C^a. Moreover, correction (35) has nearly no effect in this case ($r_r = 1$), meaning that ε is determined independently of p. One obtains $T_C^a = {}^*T_C^a(1+\varepsilon)$, i.e.

$$\varepsilon = T_C^a/\ {}^*T_C^a - 1 \tag{36}$$

$\varepsilon(\ {}^{*}T_C^a = 70\ °C) = 0.56$, $\varepsilon(\ {}^{*}T_C^a = 100\ °C) = 0.43$ are obtained.

Finally, parameters p and J_0^a are determined by seeking for the best fit of experimental curve plotted on Fig.13. Fitting procedure is carried out with the two considered ${}^{*}T_C^a$ values, leading to $p(\varepsilon = 0.56) = 8$ Å and $p(\varepsilon = 0.43) = 7.15$ Å, and same polarization $J_0^a = 0.815\ T$. Resulting fitting curves are compared on Fig. 13 to the experimental curve. The two couples of parameters appear equivalent at this stage but the couple $(\varepsilon = 0.43, p = 7.15)$ will be kept, leading to better results thereafter. Fig14 details local spontaneous magnetization profiles as a function of the distance to the interface for some temperatures in this case.

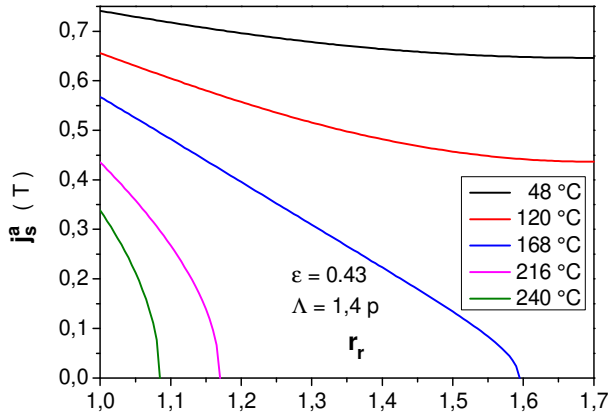

Fig. 14: Amorphous polarization depending on distance to nanograin for different temperatures

Partially crystallized samples can now be studied.

4.4 Determination of parameters for the partially crystallized state

Compared to the preceding case, some specificities featured by partially crystallized samples have to be underlined : At first, due to bigger inter-nanograin distances, correction (35) can be neglected. Secondly, Hernando [3] determined a phenomenological penetration depth which decreases as f_c increases as shown on Fig.15, with the fitted curve we adjusted. One notices that this parameter varies roughly by a factor two, from $f_c = 0$ to $f_c = 0.75$. As ε and p have equivalent effect on macroscopic properties, and taking in mind that the penetration depth we adjusted to reproduce the fully crystallized sample behavior in § 4.3 is $p_{0.75} = 7.15$ Å, we consider that, in our context, this behavior cannot be ascribed to parameter p, the extent of exchange interactions usually admitted being only several Å. Consequently, we'll apply on ε parameter this tendency. Taking in mind that we adjusted $\varepsilon_{0.75} = 0.43$ in § 4.3, we thus simply consider that the curve plotted on Fig.15 represents $10\ \varepsilon(f_c)$.

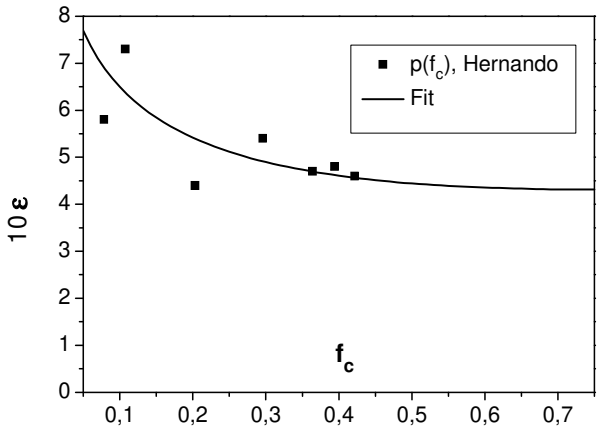

Fig. 15: ε dependence on f_c according to [3]

J_0^a and T_c^a parameters evolution as function of f_c has now to be determined. To do this, we'll simply interpolate values between extreme cases (i.e. $f_c = 0$ and $f_c = 0.75$). For fully crystallized sample $J_0^a = 0.81\ T$, ${}^*T_C^a = 100\ °C$ are already known. In order to characterize $J_s^a(T)$ law for $f_c = 0$, measurements have been carried out on a 420°C relaxed amorphous sample, plotted on Fig.16. This curve is well fitted by an Heisenberg law, with $T_c^a(f_c = 0) = 332{,}4\ °C$, but to stay consistent with modeling in the molecular field frame, another fit is considered, with an exponent 1/2. This fit is plotted in red and leads to $J_0^a = 1.28\ T$.

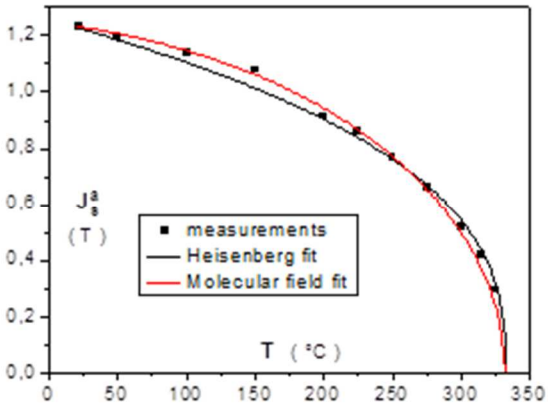

Fig. 16 Measured polarization for a 420°C relaxed amorphous sample Aperam Nanophy

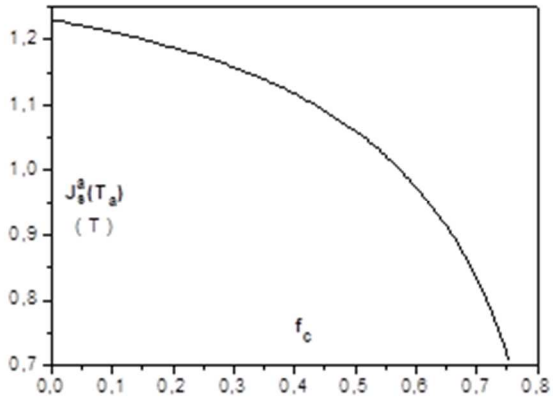

Fig. 17 Interpolated curve of the polarization of the amorphous phase

To determine interpolation function, ambient temperature polarizations are considered and corresponding parameters will be denoted with "am" superscript. Alloy and the two phases polarizations are linked by:

$$J_{s_a}^{am}(f_c) = \frac{J_s^{am} - J_{s_c}^{am}\ f_c}{1 - f_c} \tag{37}$$

In addition, thirst point of Fig.16 and Fig.11 show that $J_s^{am}(f_c = 0) = J_s^{am}(f_c = 0.75) = 1.23\ T$, in agreement with [8], considering the alloy composition used. We so consider that J_s^{am} is independent from f_c. From Fig.12 $J_{s_c}^{am} = 1.40\ T$ is determined for $Fe_{79.1}Si_{20.9}$ alloy. Is so obtained from (37)

$$J_{s_a}^{am}(f_c) = \frac{{}^0J_{s_a}^{am} + \left({}^{0.75}J_{s_a}^{am} - 4\ {}^0J_{s_a}^{am}\right)f_c/3}{1 - f_c} \quad \text{with} \quad {}^{0.75}J_{s_a}^{am} = 0.72\ T \quad and \quad {}^0J_{s_a}^{am} = 1.23\ T \tag{38}$$

The corresponding curve being plotted on Fig.17.

Equation (38) will now be generalized in order to interpolate ${}^*T_c^a$ and J_0^a parameters, leading to:

$${}^{f_c}x = \frac{{}^0x + \left({}^{0.75}x - 4\ {}^0x\right)f_c/3}{1 - f_c} \qquad x = {}_*T_C^a\ (°C)\ , J_0^a \tag{39}$$

$J_s^a(T_{tr}, r_r)$ curve associated to given f_c is thus obtained by applying relation (28) and (31), $J_0^a(f_c)$, ${}^*T_C^a(f_c)$ being defined by (36) with $({}^0_*T_C^a = 332.4\ °C\ ,\ {}^0J_0^a = 1.28\ T)$, $({}^{0.75}_*T_C^a = 100\ °C\ ,\ {}^{0.75}J_0^a = 0.81\ T)$.

4.5 Simulating results

An iterative process is used : Experimental T_{tr} given, one starts with initial value $f_c^0 = f_c^{tr}$, and with $\varepsilon_0 = \varepsilon\left(f_c^{tr}\right)$ obtained on Fig.17; $J_s^a(f_c^0, r_r)$ curve and $\langle J_s^a\rangle_0$, averaged considering the range $1 \le r_r \le 2.5$ are obtained by using relation (28) and (31). δV_1 equivalent volume, which has to be added to V in order to take amorphous phase contribution is determined by:

$$\delta V_1 = \pi\ D^2\ 1.5\ p\ \frac{\langle J_s^a\rangle_0}{J_s^c} \quad \rightarrow \quad \frac{\delta V_1}{V} = 9\ \frac{p}{D}\ \frac{\langle J_s^a\rangle_0}{J_s^c} \tag{40}$$

For simplicity we retain the constant size $= 11.6\,nm$, typical value for low f_c Nanophy® samples. Effective volume increase impact effective crystalline fraction in the same way, so (8) is modified as :

$$\frac{T_{tr}}{(1 - T_{tr}/T_C^c)^{0.72}} = C\,\frac{f_c^1\,{J_H}^2}{S_{tr}}\left(1 + 2\frac{\delta V_1}{V}\right)D^3 \qquad (41)$$

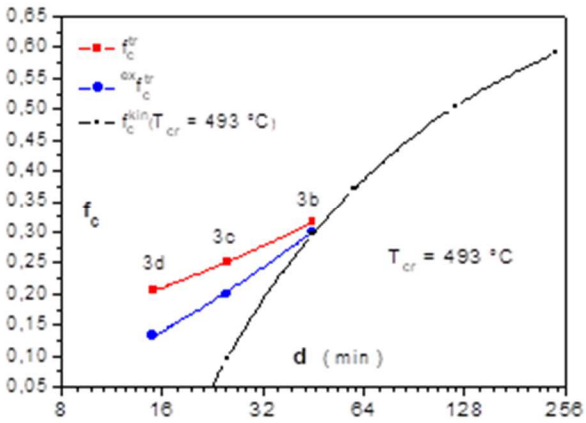

Fig.18: Crystalline fraction depending on annealing time for $T_{cr} = 493°C$, according to kinetics law (black), and transition temperature method, with (blue) and without (red) taking interphase coupling

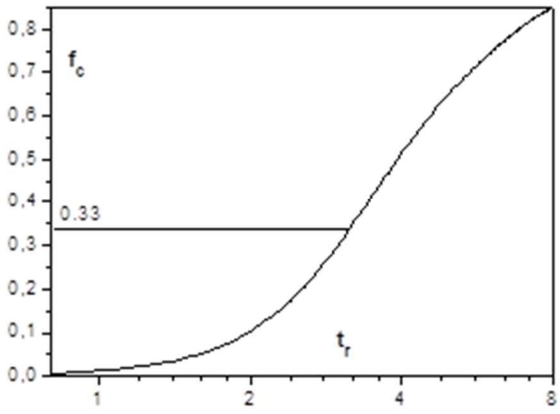

Fig.19: Crystalline fraction depending on annealing time in arbitrary units, according to [23]. Ones has to notice the incubation phase revealed by the inflexion

Equation (41) is consequently solved giving f_c^1. The same process is repeated with f_c^1 and $\varepsilon_1 = \varepsilon\left(f_c^1\right)$ as new entrances and so on, until stabilization. Table.2 is completed by final values ${}^{ex}f_c^{Tr}$ (ex for exchange) obtained by applying this method on 3b, 3c and 3d Nanophy® samples. Results are also showed on Fig.18, where ${}^{ex}f_c^{tr}$ values are compared to f_c^{tr}. Superimposed, the kinetic law obtained for $T_{cr} = 493\,°C$. The necessity of taking into account the coupling effect to determine law f_c is obvious with this figure. One has to denote that the tendency indicated by ${}^{ex}f_c^{Tr}(d)$ points are in qualitative accordance with the incubation phase described in [23] and illustrated on Fig.19. Nevertheless, coupling parameter identification is still imprecise due to lack of data about isolate amorphous. Same statement can be done about $\varepsilon(f_c)$, illustrated on Fig.15.

Finally, simulated points $(T_{tr}, {}^{ex}f_c^{tr})$ corresponding to 3b, 3c, and 3d, are added on Fig.10. Note that in case of 3b, the simulated point and experimental one (T_{tr}, f_c^{kin}), are indistinguishable. The shift featured by ${}^{ex}f_c^{tr}$ values compared to f_c^{tr} evaluations is underlined by arrows plotted on 3c and 3d points, the dashed line based on those three points providing a global view of this effect. As a result, we conclude that accounting for the interphase coupling leads to a very significant decrease of the curvature of the simulated curve $T_{tr}({}^{ex}f_c^{tr})$ compared to the $T_{tr}(f_c^{tr})$ one, providing a plausible explanation of the alignment featured by experimental points belonging to Kulik's family.

5. Conclusion

For the first time to our knowledge, modeling of the weak coupling regime in nanocrystalline samples taking account at the same time of dipolar interactions and interphase coupling, was carried out. This study was committed to determine if a new way for characterization of crystalline fraction could be proposed, based on experimental transition temperature measurements between the weak coupling regime and the super-paramagnetic one. It was shown that the influence of the interphase coupling can be neglected if $f_c > 0.3$, but has to be taken into account for lower values. In this case, strong uncertainties occur, dealing with

- the intrinsic properties of the residual amorphous phase, mainly due to the difficulty to account for the inhomogeneous distribution of Niobium
- the evolution of the ferromagnetic interphase coupling interactions with f_c.

These uncertainties impact strongly the accuracy of f_c evaluation based on T_{tr} measurement. As a consequence, the values of f_c obtained by this way are only indicative, and cannot replace, as things stands, a more direct measurement technic.

Nevertheless, from a physical point of view, and despite the lack of accuracy characterizing our treatment of interphase coupling, a robust trend emerges, that is a strong decrease of the curvature exhibited by the $T_{tr}(f_c)$ simulated curve, regarding the one obtained neglecting interphase coupling. This could explain the alignment featured by experimental points belonging to Kulik's family, curiosity unexplained until now.

Finally, this study gave us the opportunity to revisit the modelling of dipolar interactions we initiated in [14], with a strong improvement of the identification of parameters, made possible thanks to the database collected by the Aperam research center of Imphy. This modelling was mainly used regarding the transition temperature T_{tr}, but can be extended to the modelling of the spontaneous polarization in the weak coupling regime when $T < T_{tr}$, as shown in the appendix.

6. Acknowledgment

This work was supported in part by the "Association Nationale de la Recherche et de la Technologie" (convention CIFRE 2015/1098).

Appendix

The thermomagnetic study for 3a Nanophy sample in § 4.2 allows to determine polarization law $j_s^{wc}(T)$ in the weak coupling regime. Indeed, due to the applied field weakness, macrodipoles cannot align in the weak coupling behavior, i.e., in the range $T_C^a = 262\ °C < T < T_{tr} = 560\ °C$. Consequently experimental points J_{exp} are identified to j_s^{wc} instead of J_s.

Equilibrium state is solved by considering ω, given by (15), as entrance parameter. ω < 1/3 has to be considered. (5) is rewritten as

$$j_s^{wc} = \mathcal{L}[x] \qquad (A1) \qquad with \qquad x = j_s^{sc}/\omega \qquad (A2)$$

So $$\mathcal{L}[x] = \omega\, x \qquad (A3)$$

ω being given, x is determined with (A3) and j_s^{wc} with (A1).

j_s^{wc} being different from 0, it should be taken $h_{a\chi} = \langle \left\| \vec{h}_{sh}^{r} + \vec{h}_{sh}^{ca} \right\| \rangle$ to determine the amplitude susceptibility featured by the shell, brackets indicating an angular average on the shell, $\vec{h}_{sh}^{r}$ and $\vec{h}_{sh}^{ca}$ obeying (10) and (11). For simplicity, we consider that $\vec{h}_{sh}^{r}$ is majority and neglect thus contribution due to $\vec{h}_{sh}^{ca}$. (18) is so generalized for $T \leq T_{tr}$ leading to :

$$h_{a\chi} = A\, f_c / (3 + 2\chi) \qquad (A4)$$

$h_{a\chi}$ is replaced in (16) by its expression (A4), leading to

$$A\,(3 + \chi) / (3 + 2\chi) = \omega\, x_\chi \qquad (A5)$$

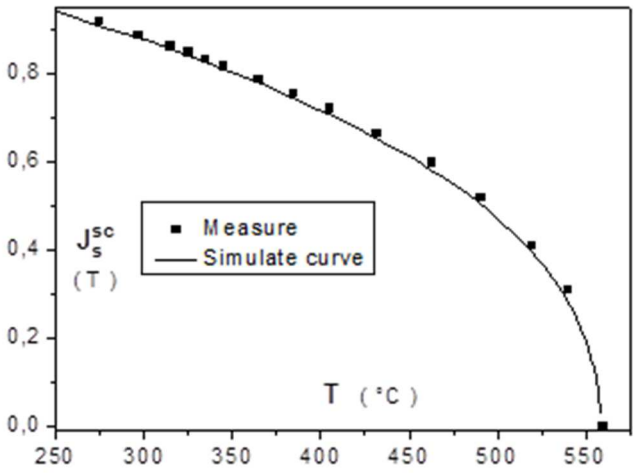

Fig.A1: Measured spontaneous polarizations in the weak coupling regime for 3a fully crystallized Nanophy® sample compared to simulated curve

An equation in x_χ is obtained by replacing χ using (14). The x_χ value obtained solving this equation is injected in (14), giving χ value. In (15) relation, J_s is replaced by its (7) expression and S by its (9) expression, giving

$$\omega = \frac{1}{27\,S_{tr}} \frac{(3+\chi)(3+2\chi)}{1+\chi} \frac{(T_C - T_{tr})^{0.72}}{(T_C - T)^{0.72}} \frac{T}{T_{tr}} \qquad (A6)$$

χ, S_{tr} and T_{tr} are known and their values injected in (A6). Solving (A6), T is obtained, allowing to determine $J_s$through (7) and so $J_s^{wc} = j_s^{wf} J_s$. (T, J_s^{wc}) couple is so determined.

The simulated curve is successfully compared to experimental one on Fig.A1.

BIBLIOGRAPHY

[1] Zs. Gerci, F. Mazaleyrat, and L.K. Varga, *High-temperature soft magnetic properties of Co-doped nanocrystalline alloys*, J. Mag. Magn. Mat. 302 p.p. 454-458 (2006)

[2] G. Herzer, *Grain Structure and Magnetism of Nanocrystalline Ferromagnets*, IEEE Trans on Mag 25, pp. 3327-3329 (1989)

[3] A. Hernando, I. Navarro and P. Gorria, *Iron exchange-field penetration into the amorphous interphase of nanocristalline materials*, Phys. Rev. B 51, 3281 (1995)

[4] A. Slawska-Waniewska, M. Gutowski, and H.K. Lachowicz, *Superparamagnetism in a nanocrystalline Fe-based metallic glass,* Phys. Rev. B 46, 14594-14598 (1992)

[5] A. Slawska-Waniewska, P. Didukh, H.K. Lachowicz, and T. Kulik, *Microstrctural transformation and magnetic properties of annealed CoNbCuSiB alloy,* J. Mag. Magn. Mat. 215-216 pp. 495-498 (2000)

[6] L. Varga, F. Mazaleyrat, G. Kovacs, and A.Katay, *The role of the residual amorphous matrix in determining the temperature dependence of soft magnetic properties of nc alloys,* J. Mag. Magn. Mat. 226-230, pp. 1550-1552 (2001)

[7] T. Kulik and A. Hernando, *Magnetic properties of two-phase nanocrystalline alloy determined by anisotropy and exchange interactions through amorphous matrix*, J. Mag. Magn. Mat. 138 270-280 (1994)

[8] G. Herzer, *Nanocrystalline soft magnetic alloys*, Handbook of Magnetic Materials, vol.10, Buschow, 1997

[9] A. Hernando, P. Marin, M. Vazquez, J.M. Barandiaran, and G. Herzer, *Thermal dependence of coercitivity in soft magnetic nanocrystals*, Phys. Rev. B 58, pp. 366-370 (1998)

[10] P. Marin, C. Gomez-Polo, and A. Hernando, *Magnetism of two-phase magnetic systems composed of nanograins embedded in an amorphous matrix*, Mat. Sci. Eng. A 449-451, pp. 71-78 (2007)

[11] A. Hernando, and T. Kulik, *Exhange interactions through amorphous paramagnetic layers in ferromagnetic nanocrystals*, Phys. Rev. B **49**, pp. 7064-7067 (1994)

[12] S. Morup, M.F. Hansen, and C. Fransen, *Magnetic interactions between nanoparticles*, Beilstein J. Nanotechnol 1 pp. 182-1909 (2010)

[13] G. Herzer, *Soft magnetic nanocrystalline materials*, Script. Met. Mater. 33, pp. 1741-1756, 1995

[14] O. Geoffroy, H. Chazal, Y. Yao, T. Waeckerle, and J. Roudet, *Modelization of superferromagnetism in soft nanocrystalline materials based on an accurate description of magnetostatic interactions*, IEEE Trans. Magn., 50, pp. 1-4 (2014)

[15] Yunxia Yao, "Etude des matériaux magnétiques nanocristallins FeCuNbSiB pour applications en électronique de puissance", Phd Thesis Grenoble Alpes University 2015

[16] J.C. Maxwell, *Electricity and Magnetism*, II, Clarendon Press, 1873 p. 58, available at http://gallica.bnf.fr/ark:/12148/bpt6k95176j/f84.image

[17] H. Fröhlich, *Theory of dielectrics*, Oxford Science Publications, second ed. 1957

[18] L. Onsager, *Electric moments of molecules in liquids*, *J. Am. Chem. Soc.* 58, p. 1486, 1936

[19] S. N. Kane, S. S. Khinchi, F. Mazaleyrat, Z. Gercsi, A. Gupta, and L. K. Varga, *Study of structural and magnetic properties of Co-substituted* $(Fe_{100-x}Co_x)_{78}Si_9Nb_3Cu_1$ *alloys*, J. Phys., Conf. Series 144 012078 pp.1-4 (2009)

[20] F. Mazaleyrat, and L.K. Varga, *Thermo-Magnetic Transitions in Two-Phase Nanostructured Materials,* IEEE Trans on Mag 37, pp.2232-2235 (2001)

[21] M. E. McHenri, M. A. Willard, and D. E. Laughlin, *Amorphous and nanocrystalline materials for applications as soft magnets*, Progr. Mat. Sci. 44 pp. 291-433 (1999)

[22] H. A. Shivaee, and H. R. M. Hosseini, *Advanced isoconversional kinetics of nanocrystallization in* $Fe_{73.5}Si_{13.5}Nb_3Cu_1$*alloy*, Thermochimica Acta 494 pp. 80-85 (2009)

[23] T. Pradell, D. Crespo, N. Clavaguera et M. Clavaguera-Mora, *Diffusion controlled grain growth in primary crystallization: Avrami exponents revisited, J. Phys. Condens. Matter.* 10, pp. 3833-3844 (1998)

[24] R. Skomski, *Simples Models of Magnetism*, Oxford University Press (2008)

[25] S. Chikazumi, Physics of magnetism, Wiley and Sons (1964)

[26] M. Fallot*, Ferromagnétisme des alliages de fer*, Phd thesis, faculté des sciences de l'université de Strasbourg, 1934.

[27] A. Slawska-Waniewska, M. Gutowski, and H.K. Lachowicz, *Superparamagnetism in a nanocrystalline Fe-based metallic glass,* Phys. Rev. B 46, 14594-14598 (1992)

[28] C. Kurt, and G. Herzer, *The Residual Amorphous Phase in Nanocrystalline Soft Magnetic FeSiCuNbB*, IEEE Trans on Mag 32, pp. 4881-4883 (1996)

[29] R. Yavari, *Nanocrystallization of Fe-based soft-magnetic amorphous alloys*, "Nanostructured and non-crystalline materials", M. Vazquez and A. Hernando eds, World Scientific, 1994